Crack Monitoring using Short-gauged Brillouin Fiber Optic Sensor

Citation for published version:
Han, T, Wu, G & Lu, Y 2021, 'Crack Monitoring using Short-gauged Brillouin Fiber Optic Sensor', *Measurement*, vol. 179, 109461, pp. 1. https://doi.org/10.1016/j.measurement.2021.109461

Digital Object Identifier (DOI):
10.1016/j.measurement.2021.109461

Link:
Link to publication record in Edinburgh Research Explorer

Document Version:
Peer reviewed version

Published In:
Measurement

Crack Monitoring using Short-gauged Brillouin Fiber Optic Sensor

Tianran Han [a,b], Gang Wu [a,b,*], Yong Lu [c]

[a] *National and Local Joint Engineering Research Center for Intelligent Construction and Maintenance, Nanjing 211189, China*

[b] *Key Laboratory of Concrete and Prestressed Concrete Structures of the Ministry of Education, Southeast University, Nanjing 211189, China*

[c] *Institute for Infrastructure and Environment, School of Engineering, The University of Edinburgh, Edinburgh EH9 3JL, UK*

Abstract

Detection and quantification of cracks for various civil infrastructures on a large scale are difficult both technologically and economically through current sensing methodologies. This study presents a novel fiber-optic sensor named short-gauged Brillouin fiber optic sensor, which enables basic Brillouin-based analyzers to achieve early crack detection and accurate crack width measurement. The concept and design of the proposed sensor are firstly introduced, followed by respective instrumentation procedures. On this basis, theoretical deduction and numerical simulations of the crack-induced Brillouin gain spectrum (BGS) response using the proposed sensor are carried out, verified subsequently by controlled laboratory tests. The measured BGS responses are then leveraged for crack detection and quantification. A peak-fitting-based methodology was adopted to analyze the BGS data to achieve accurate crack width measurement. The proposed methodology may facilitate economical long-distance distributed crack sensing and quantification for various infrastructures as a genetic technique.

Keywords: distributed fiber optic sensing, crack sensing, short-gauged Brillouin fiber

optic sensor, crack width measurement

1. Introduction

Crack formation is a common form of structural degradation in civil infrastructure due to aging, fatigue, unfavorable loading, or environmental processes [1]. Crack development in structures inevitably affects the infrastructure in terms of its functionality, aesthetics, durability, and even safety. For reinforced concrete (RC) structures, when crack opening exceeds a certain level (0.2 to 0.4 mm depending on environment), the corrosion process of steel reinforcement within the structures may be accelerated by chemical ingression, thus adversely affecting structural durability. Larger cracks in the order of 1 mm or greater could indicate severe damage in the structures that may require immediate attention for retrofitting [1, 2]. Therefore, awareness and assessment of the in-place cracks are crucial for various infrastructure structural elements.

However, early-stage structural cracks are small and often take place randomly in a sporadic distributive manner. Compounded with the size and scale of the infrastructure systems, these make detection of early-stage cracks particularly difficult and even harder for quantification. Monitoring options that can tackle large-scale crack detection and quantification problems, and do it economically, could produce crucial information for timely preventive structural maintenance, leading to prolonged service life and reduced maintenance costs in life-cycle management.

In engineering practice, the acquisition of crack information has conventionally relied on periodic visual inspections, which can be time-consuming, expensive, and unreliable. While various nondestructive testing (NDT) techniques may be used to facilitate the examination for structural damages or cracks, they share the difficulty of accurately measuring crack openings and render real-time evaluations for the structural status [3].

On the other front, sensors capable of continuous monitoring in time, such as strain sensors (electrical or fiber Bragg grating) are typically discrete or quasi-distributive sensors that can only detect cracks if they occur at immediate proximity of the sensing locations. Such sensors tend to suffer from possible miss detection of cracks, and extensive scale application of these types of sensors will be constrained by the high sensor costs and the hosting capacity of the analyzers [4, 5].

Although distributed fiber optic crack sensing can be realized using signal-loss-based methods based on OTDR (Optical Time Domain Reflectometer) [6, 7]. These applications usually involve orchestrating special zigzag sensor installation schemes and can be challenging to achieve long-range monitoring due to the potential depletion of the light power budget along the sensing fiber. Likewise, the Rayleigh-scattering-based technique, which has recently grown in popularity, can achieve high spatial resolution (smaller than 10 mm) but at the cost of a short achievable measurement range (upper limits within 100 meters). As such, their application has been primarily limited to laboratory tests [8, 9].

Brillouin-based fiber-optic distributed sensing is a promising technology for long-range deformation monitoring of many types of infrastructure such as bridges

[10, 11], pipelines [12, 13], tunnels [14]. The technology enables retrieval of continuous measurement of strain for structures up to tens of kilometers.

Studies have been carried out in crack and deterioration sensing using Brillouin fiber optic sensors, valuing their fully distributive nature to achieve a higher likelihood of intersecting potential cracks. Those sensing methods customarily rely on searching for spikes in the distributed strain profiles obtained by the sensing systems [15, 16]. However, with the standard options of commercially-available Brillouin sensing systems, the best achievable spatial resolution (SR) is often in the order of 0.5 to 1.0 m, which is apparently a significant drawback when it comes to crack or deterioration detection where information of localized deformation is of interest. SR defines the smallest length corresponding to strain events that can be measured with defined or targeted accuracy [17]. An experimental study involving a 15-m-long beam showed that the strain localization due to structural defects tended to be masked by the low spatial resolution effect of the Brillouin analyzer, making the distributed strain measurement insensitive to the crack formation[18]. Consequently, the sensing measurement was neither capable of accurately localizing the defects nor capable of indicating their severity via the measured strain amplitudes.

In coping with the unfavorable effects from low SR of the Brillouin analyzer on crack detection, a signal-processing approach was described based on the decomposition of the distributed strain data from BOTDR (Brillouin optical time-domain reflectometer) using the stationary wavelet-transform method. It achieved improved crack features and enhanced data quality [19]. However, this method requires a dense spatial sampling rate from the analyzer along the measurement fiber, which may not be commonly available, and the specific wavelet function and determination of the vanishing moment may differ for different problems. Another attempt involved a data processing methodology using the maximum compressive or tensile peaks in the Brillouin frequency spectrum to obtain the distributed strain instead of the distributed strain obtained by conventional methods [20]. As such, enhanced sensitivity was achieved for crack detection. However, these methods cannot be used to quantify crack width accurately. Quantification for crack sizes and numbers based on distributed strain has relied primarily on statistical and empirical approaches, such as proposing quantitative empirical parameters and relating them to many experimental observations [21], rendering crack assessment on a case-by-case basis. Understandably, crack formation will introduce complicated strain distribution to the distributed fiber optic sensors, which will create distortions to the Brillouin gain spectrum (BGS) [21, 22]. A Brillouin-based crack sensor was developed capable of detecting cracks less than 1 mm in width, and a sensor installation technique was devised using specialized glue to avoid sensor breakage as crack occurs [23]. The sensor relies on redistribution of crack-induced strain through partial sensor detachment from the attached structure to achieve crack detection by examining the respective spectrum feature. However, the mechanical interface behavior may possess a considerable degree of variation in relation to crack opening based on specific interfacial conditions. Tests revealed that the detachment could only happen when relatively large cracks occur. Therefore, while the methodology enabled detecting relatively large cracks (in the order of 0.5 mm or more), it is also difficult to obtain accurate crack quantification [24].

To quantitatively assess cracks, long-gauge distributed fiber optic sensors (gauge length greater than SR of the analyzer) were adopted along with several other unique installation methods involving the usage of acrylic disk guides[25]. Their effectiveness in measuring total crack width within a particular structural region through strain-displacement conversion was verified by reinforced concrete (RC) beam testing. However, these long-gauge arrangements would only obtain the averaged crack width information, likely missing the detailed information for individual cracks. It would also be difficult to tell if the measured strain increments indeed arise from the crack formation. Besides, the installation methods involving superposition loops can be complex to apply in the field.

Another way to obtain a more sensitive crack-sensing capability for the Brillouin fiber optic strain sensors relies on directly improving the SR of the analyzers. Although directly decreasing the pump pulse duration could supposedly improve the spatial resolution, it comes at a price of lowered signal-to-noise ratio (SNR) and thus decreased accuracy of sensor sensitivity, thereby practically limiting the spatial resolution to about 1 m. Some similar special techniques have been proposed to achieve higher SR, and at the same time, avoid compromising the strain resolution. For instance, Differential Pulse-width Pair BOTDA (Brillouin optical time-domain analysis) [26], Pump pre-pulse BOTDA [27], Gain-Profile Tracing BOTDA [28], and other techniques involving ‘Bright pulse’ [29], ‘Dark pulse’ [30] or ‘Brillouin echoes’[31]. The common basis of these techniques is the pre-excitation of the acoustic field. While some of these techniques can facilitate the attainment of SRs in the order of several centimeters, enabling crack sensing capacity for micro-cracks

[32], expenses always follow at other aspects, such as the requirement for long time measuring, shorter sensing length, increased system sensitivity to noises, more sophisticated and sensitive systems which are rarely commercially available and often expensive.

In order to achieve accurate measurement of cracks, another hurdle exists besides the SR-related issues of the Brillouin analyzer-it is essential to understand the crack-induced strain transfer mechanisms between the cracked structures and the fiber optic sensors. The traditional approach of distributed fiber optic strain sensing aiming for crack or deterioration detection has primarily relied on overall bonding (OB) the sensing cables to the monitoring structures, such as in the cases of concrete beams [20, 33], bridges [11], and pipelines [12, 16]. Although linear elastic response can be derived in coping with tiny cracks [32], this underlying assumption inevitably limits the prediction accuracy when nonlinear responses come into play. Extensive research suggests that the crack-induced strain transfer in fiber optic sensors is a highly complex and variable phenomenon that involves different types of nonlinearities, such as detachment, plasticity, and slippage between substrata layers, depending on specific fiber optical sensor design, gel properties, installation methods, and characteristics of the monitored structures [8]. Therefore, considerable difficulties exist in reaching a generic crack quantification solution that can cope with cracks of various sizes, from different origins, and for multiple applications, using the standard sensor instrumentation technique.

This study presents a novel fiber-optic sensor concept and design named short-gauged Brillouin fiber optic sensor, which enables basic Brillouin-based analyzers to detect and accurately quantify events of cracks or structural discontinuities. The short-gauged Brillouin fiber optic sensor may potentially facilitate the attainment of economical long-distance distributed crack sensing and quantification for Structural Health Monitoring (SHM) of various infrastructures. The proposed sensor can become a powerful generic crack sensor capable of crack early warning through identifying distinctive crack signatures and accurate crack-width measurement, minimizing uncertainties from different fiber and adhesive properties and instrumentation details where the traditional OB instrumentation approach usually confronts. The proposed instrumentation method also constructs a new way to deploy distributed fiber optic sensors, besides the traditional overall bonding and point-fixation (long-gauge) approach.

The paper starts by introducing the concept, design, and installation scheme of the proposed sensor. Afterward, theoretical deduction and numerical simulations of the BGS response due to crack propagation, using the proposed sensors, are carried out. The results demonstrate the characteristics of the BGS transformation in different evolutional stages as the crack propagates, which are then verified by a controlled laboratory test. Finally, the effectiveness of using the proposed sensors as crack meters is studied and discussed by extracting the crack information via proper data processing of the experimental data.

2. Short-gauged Brillouin fiber optic sensor: concept and design

For distributed fiber optic sensors, two different installation techniques usually apply in practice, namely the overall bonding (OB) method and the point-fixation (PF) method [25]. The OB method continuously attaches the fiber optic sensors to the structure being monitored via adhesives or through embedment, while the PF method only fixes the fibers to the structure at discrete locations by anchorage points spaced at specific intervals. This spatial interval between the anchorage points is termed gauge length (GL), as shown in Fig. 1.

Both of these methods have been extensively implemented in the monitoring practice [14, 34, 35]. For example, the OB installation method was applied in tunnel SHM projects to assess the shield tunnel lining’s cross-sectional performance in Barcelona[35] and London[14]. Likewise, a field trial utilizing PF installation method to monitor an existing tunnel’s distortion movement due to the adjacent new tunneling activities was reported [34]. The PF was achieved by attaching an optical fiber around the circumference inside the tunnel linings using wheels. The OB method could potentially preserve the detailed distributed deformational information of the monitored structures; however, due to the complex nature of the strain transfer mechanism, extraction of local deformational information can often be tricky. Further, discontinuities in the structure, such as cracks, may render fiber optic cable to fracture, causing the sensing system to fail. On the other hand, the PF method usually takes the form of a long-gauge arrangement, providing average strain information between the fixation points, which can, in general, provide straight-forward strain-displacement conversions. The PF method also tends to be free from the risks of crack-induced cable ruptures due to avoidance of exceedingly large local stress in the fiber. For field applications, the gauge length adopted for the Brillouin sensor using PF installation ranges typically in the order of 0.5 to 2 meters, depending on specific applications. In regular practice, assurances are guaranteed that the fiber optic sensor's gauge length shall be greater than the SR of analyzers for enhanced sensing system repeatability and easier on-site sensor instrumentation. However, due to the long-gauge arrangement, information loss is inevitable of the detailed strain distribution between fixation points. Moreover, for most applications, the achievement of point fixation relies on accurate positioning and installation of anchorages on site, which can be time-consuming.

In light of the shortcomings of the conventional installation techniques, we hereby propose a novel fiber-optic sensor concept and design that could potentially facilitate the retrieval and quantification of critical localized deformation beneath the analyzer's SR level when proper data processing methodologies are introduced. The key idea is to come up with a fiber optic sensor concept that could achieve a densely spaced array of strain measurements below the analyzer's SR, with a sufficiently simple relationship of strain-displacement conversion within the sensor, so that localized structural deformation will transform into a salient local strain of the sensor in a fully controlled manner. As such, crack information can be extracted with much ease.

We hereby define a sensor concept named short-gauged Brillouin fiber optic sensor (SGB-FOS). The SGB-FOSs are fiber optic strain sensors discretely spot-fixed to the monitored structure with sensing GLs smaller than half of the SR of the adopted Brillouin analyzers. The extraction of the crack quantification information will be relying on analyzing the Brillouin gain spectrum (BGS) responses. We define the GLs to be smaller than half of the analyzer's SR so that the crack-induced BGS evolutional process could form a consistent pattern with sensitive crack signatures for further data processing. Details of this will be illustrated in later sections. This concept will result in sensor GL in the order of 50 mm to 500 mm for typical commercially available Brillouin fiber-optic analyzers (basic BOTDAs and BOTDRs), depending on their achievable SRs. The specific choice of the sensor GL depends on the purpose of monitoring and the type of monitored structure. For example, it might be appropriate to select a gauge length close to or slightly smaller than the expected crack intervals of RC structures for crack quantification.

The spot-fixation arrangement of the SBG-FOS allows a fully controlled strain-displacement conversion. Specifically, the strain generated between the anchorage points in the sensor will resemble a uniform distribution instead of much more complicated distributions within OB sensors. This avoids unnecessary nonlinear response at the sensor level. The spot-fixation arrangement also tends to make the sensing system more robust against localized large deformation due to avoidance of extreme strains that could lead to fiber ruptures. Furthermore, the spot-fixation arrangement makes sensing of the local strain reversible, meaning that not only crack expansion but its closure can be equally measured.

Fiber optic sensors using PF installation can be tricky to install in practice due to the difficulty of creating a densely-spaced array of anchorages along the fiber optic sensors. Therefore, good sensor design and installation procedures are vital to make the SBG-FOS concept applicable in practice.

We hereby exemplify a sensor design that enables an easy short gauge formation in the sensor installation process. The proposed sensor design comprises a standard tight-buffered strain-sensing cable and a unique outer tubing sleeve, forming a flexible simple-structured cable sensor. The inner sensing cable is free to slide inside of the outer sleeve. The sensing cable adopts G652D single-mode optical fiber with the core and cladding measured 9.5 μm and 125μm in diameter, respectively. The coating and buffer are made of soft plastic and polyamide with an outer diameter of 0.9 mm. The sleeve with an inner diameter of 1.5 mm is composed of an inner stainless steel strangle layer and an outer plastic layer. The sleeve tubing exists for two main functions: protecting the internal sensor and forming a short-gauge arrangement. The stainless steel strangle layer provides necessary strength sheltering against possible mechanical impacts and achieving high durability against corrosions. The short-gauge arrangement is pre-formed through sensor fabrication by open windows discretely at the design gauge length in the outer plastic layer of the tubing sleeve. Fig.1 schematically shows details of the proposed sensor.

During the field deployment, the outer sleeve is segmented into 10-20 meter sections to facilitate easier handling. After properly cleaning the structural surface, the proposed sensor is first attached to the monitoring structure surface by gluing the sleeves sparsely in the plastic-covering zones. After this, one end of the internal strain sensor is point-glued to the structure by fast glue or otherwise fastened by clamps. After the anchorage becomes effective, pre-stress is applied sequentially to the internal sensing cable until the complete coverage of the sensor is under stress. The conservation of the pre-stress is ensured by timely fixing the other end of the internal sensing cable to the structure, either by glue or clamps as anchorages. The procedure to pre-stress the strain-sensing cable on site, is to the greatest extent, attempting to generate a uniform initial strain distribution within the fiber optic sensor, which is essential for crack identification at the later stage.

The pre-stress enables the sensor to detect compressive deformation of the structure. The magnitude of the pre-stress should be chosen according to the specific application and fiber optic sensors. In our installation, the fibers are generally pre-strained to around 3000 με. Care should be taken on-site to prevent dust and dirt from penetrating the sensor in the installation stage, which can be achieved by providing certain coverage or protection before the pre-stressing process. After pre-stressing, a special gel is applied to cover the sensor, gluing it to the structure entirely. Meanwhile, short-gauged anchorages are automatically formed due to gel penetration through the windows in the sensor sleeves to the internal strain cable. The gel is epoxy-resin-based, specially developed through a series of laboratory tests to possess optimized viscosity and working time, which enable it to penetrate the sensor sleeves, stably glue the sensors to the structure and accurately stay in the window area without spreading to the unintended region of the internal sensor. After hardening, the gel provides another effective protection layer for the sensor against potential detrimental environmental impacts. Additional protection should be provided for the exposed fiber regions. Fig.1 and Fig.2 demonstrate the design and instrumentation procedure of the proposed sensor. Fig.3 illustrates an example of the SGB-FOS application inside an operational shield metro tunnel to assess the tunnel lining structures' long-term circumferential structural performance. The tunnel is buried in the Eastern China soft ground, being disturbed by some nearby construction activities. The instrumentation of the sensors was carried out at mid-night time windows after all train operations were stopped. The installation of the proposed sensor inside the tunnel was proved to be convenient and fast.

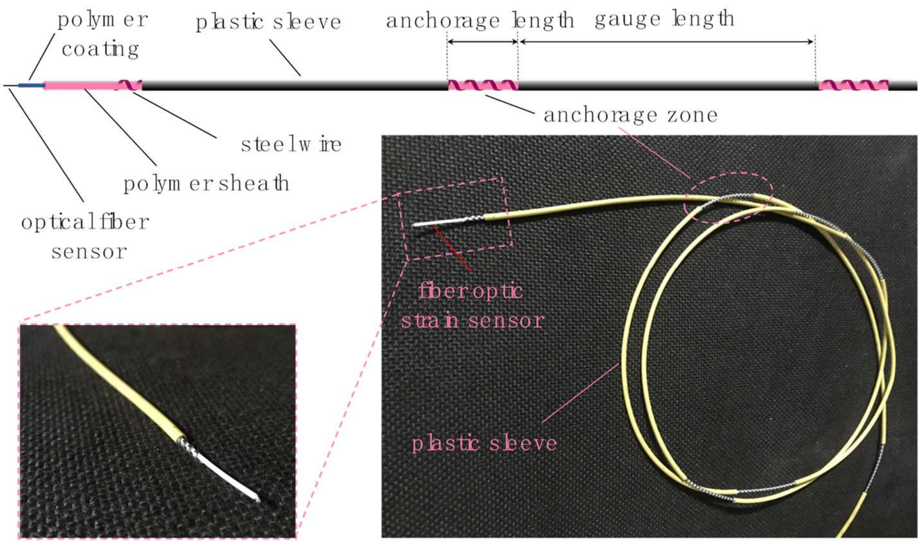

Fig.1. Distributed short-gauged Brillouin fiber optic sensor.

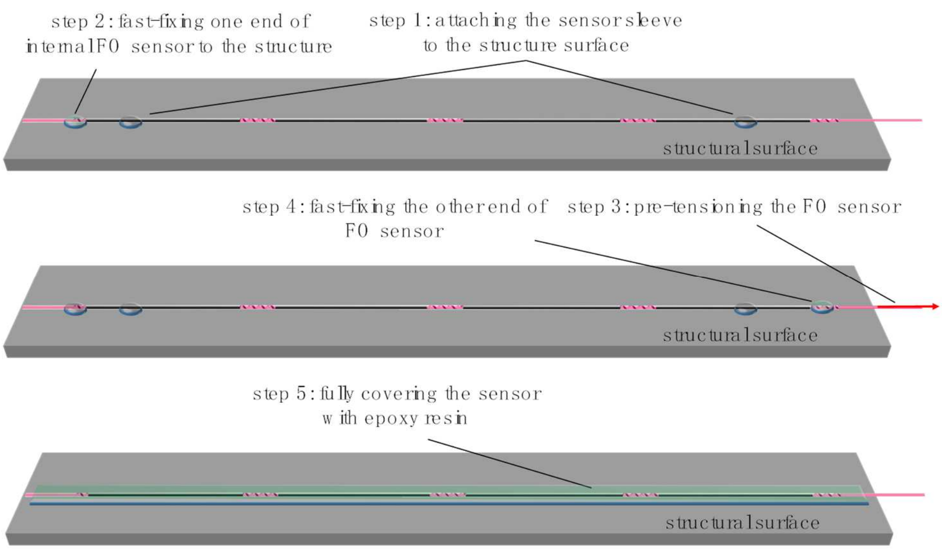

Fig.2. SGB-FOS installation procedures.

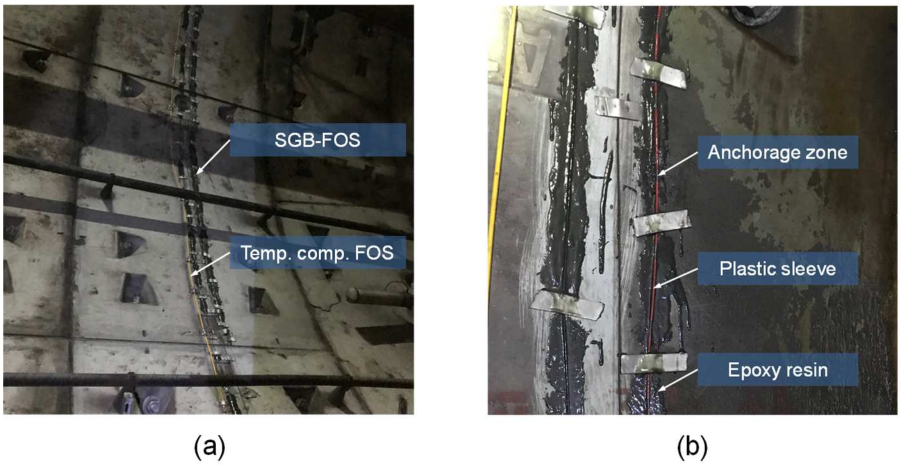

Fig.3. Example of SGB-FOS installed inside a shield metro tunnel: (a) instrumentation of the SGB-FOS for tunnel cross-sectional SHM; (b) the close-up view of the installed SGB-FOS on tunnel lining.

3. SGB-FOSs for crack sensing: theory and numerical simulation

As crack forms, the concentrated strain will occur in the proposed fiber optic sensor. This crack-induced strain is generally much larger than the strain at uncracked structural sections. For example, a 0.2 mm crack would introduce a 2000 με in an SGB-FOS of 100 mm GL, which can be one order greater than the background strain of uncracked sections. This major sub-spatial resolution event will distort the shape of the BGS profile from the standard one when the strain within the SR is uniformly distributed. Therefore, the extraction of the Brillouin frequency shift (BFS) adopted by the analyzers through standard peak fitting procedures will render significant error, thus no longer suited to accurately extract the quantitative information of the crack

[36, 37]. Therefore, a theoretical framework of the BGS evolution with crack propagation using the proposed fiber optic sensor should be established.

3.1. Crack-induced strain in SGB-FOSs

Due to the spot-fixation arrangement, the strain transfer mechanism between the structure and the short-gauged fiber optic sensor is considerably simplified. As a crack occurs, the crack displacement will translate into a spiking localized strain between anchorage points of the sensor bridging over the crack. For simplicity, we assume that the crack-induced strain is uniformly distributed within a certain gauge length, featuring a prominent rectangular peak. Although there exist transient regions for the strain to build up from the background strain to the rectangular peak, we can approximate this effect by introducing a nominal gauge length to cope with their influence on the BGS response (see Fig. 4). Theoretically, this nominal gauge length is always greater than the fiber optic sensors' design gauge length.

Let k_1 denote the ratio of the design gauge length (GL_d) to the nominal gauge length (GL_n), which is a value of less than 1.0 (see Eq.1). Also, due to the shear lag in the substrata of the fiber optic sensors, the strain transfer from the crack displacement to the optical fiber core can never be 100%. Therefore, the measured strain from the fiber optic sensor will always be smaller than that from direct crack width (d) conversion. This effect is indicated by a strain transfer factor k_2, which is also a factor smaller than 1.0. The specific values of k_1 and k_2 may rely on various factors, such as the strain sensing cable, fixation methods, and gauge length. Individual estimation of the exact values of k_1 and k_2 would require detailed material qualities of the fiber optic sensor or via refined experimental measurements capable of obtaining high-SR distributed strain using, for example, the Rayleigh-scattering-based strain measuring technique. However, their effect for crack strain evaluation can be represented by a combined factor k, which could be obtained experimentally. Therefore, the crack induced strain (ε_c) for the short-gauge sensor can be formulated in equation (2).

$$k_1 = GL_d / GL_n \tag{1}$$

$$\varepsilon_c = k_2 d / GL_n = k_2 d / GL_n = k_1 k_2 d / GL_d = kd / GL_d \tag{2}$$

3.2. Modeling the measurement system

The proposed sensor is based on the Brillouin nonlinear process that takes place in single-mode optical fibers. The most commonly used Brillouin fiber optic interrogation systems are BOTDA and BOTDR, which employ the principles of stimulated Brillouin scattering and spontaneous Brillouin scattering, respectively. The proposed crack sensing methodology can be applied to both of these systems. However, for the theoretical introduction, we will base our discussion on BOTDA systems.

In stimulated Brillouin scattering (SBS), the interference of the forward propagating pump wave (A_{pump}) and the backward propagating probe wave (A_{probe}) creates a moving optical intensity wave. Due to the phenomenon of electrostriction, the moving intensity wave induces a corresponding acoustic wave (Q) moving in the same direction as the pump. The generation efficiency of the acoustic wave depends on the relative magnitude of the pump-probe frequency offset (v_a) and a characteristic frequency shift called Brillouin frequency shift (v_B), which is a function of the local temperature and mechanical stress in the fiber. The maximum growth of the acoustic wave is reached provided v_a equals to v_B. Due to the elasto-optic effect, the optically-induced acoustic wave functions as a moving refractive Bragg grating. Coupled with the Doppler effect, this moving Bragg grating is responsible for a coherent power transfer that results in a net gain of the probe and net loss of the pump for Stocks process.

Mathematically, the assumed co-polarized, but counter-propagating pump (A_{pump}) and probe (A_{probe}) waves generate an acoustic field (Q), which couples the two optical fields. The propagation of these three waves is governed by [38]

$$\frac{\partial A_{pump}(z,t)}{\partial z}+\frac{1}{V_g}\frac{\partial A_{pump}(z,t)}{\partial t}=i\frac{1}{2}g_2 A_{probe}(z,t)Q(z,t)-\frac{\alpha}{2}g_2 A_{pump}(z,t) \quad (3)$$

$$\frac{\partial A_{probe}(z,t)}{\partial z}-\frac{1}{V_g}\frac{\partial A_{probe}(z,t)}{\partial t}=-i\frac{1}{2}g_2 A_{pump}(z,t)Q^*(z,t)+\frac{\alpha}{2}A_{probe}(z,t) \quad (4)$$

$$\frac{\partial Q(z,t)}{\partial t}+\Gamma_A Q(z,t)=ig_1 A_{pump}(z,t)A^*_{probe}(z,t) \quad (5)$$

$$\Gamma_A=2\pi i\frac{v_B^2-v^2-iv\Gamma_B/2\pi}{2v} \quad (6)$$

where g_1 and g_2 represent the electrostrictive and elastooptic coupling effects, respectively. Γ_B is the acoustic damping constant and α is the logarithmic optical loss in the fiber.

When the pump and probe powers are kept weak enough so that small-signal gain holds and pump depletion is avoided, the evolution of the amplitude $A_{probe}(z)$, and power, $P_{probe}(z)$, (in Watt), for a backward propagating CW probe, over a segment of fiber with length L can be obtained as

$$A_{probe}(z)=\left|A_{probe}(z=L)\right|\exp\left[\frac{g_1 g_2\left|A_{pump}\right|^2}{2}\mathrm{Re}\left(\frac{1}{\Gamma_A}\right)(L-z)+\frac{\alpha}{2}(L-z)\right]$$
$$\times\exp\left[i\frac{g_1 g_2\left|A_{pump}\right|^2}{2}\mathrm{Im}\left(\frac{1}{\Gamma_A}\right)(L-z)\right] \tag{7}$$

and

$$P_{probe}(z)=P_{probe}(z=L)\exp\left[g(v)P_{pump}(L-z)/A_{eff}-\alpha(L-z)\right] \tag{8}$$

where A_{eff} is the effective area of the fiber core. The logarithmic Brillouin gain, g (ν), is given by:

$$g(v=v_{pump}-v_{probe})=g_1 g_2\,\mathrm{Re}[\frac{1}{\Gamma_A}]\xrightarrow{\Delta v_B<<v_B} g_B\frac{(\Delta v_B/2)^2}{(v-v_B)^2+(\Delta v_B/2)^2} \tag{9}$$

which takes the line shape of a Lorentzian profile with a peak gain of $g_B = 2g_1g_2/\Gamma_B$ and a full width at half maximum (FWHM) linewidth of $\Delta\nu_B = 1/(2\pi\tau_A)$. Typically, for standard single-mode optical fibers at around 1550 nm, $\nu_B \sim 11\ \mathrm{GHz}$, $\Delta\nu_B \sim 30\ \mathrm{MHz}$, $g_B \sim 2-3\times10^{-11}\ \mathrm{m/W}$, $\alpha = 0.2\mathrm{dB/km}$, $\mathrm{A}_{eff} = (50-80)\times 10^{-12}\mathrm{m}^2$ [39].

Equation (9) characterizes the spectrum shape from the interaction of a CW pump and probe. However, for standard BOTDA in structural monitoring, the pump is modulated as a pulse to achieve a certain SR for discerning localized information along the fiber. The SR is determined by the pump pulse half duration multiplied by the group velocity of the guided mode [36]. Mathematically, the following formula is given,

$$SR = TV_g/2 \tag{10}$$

As the pump is pulsed, the BGS can be obtained from the convolution of the Lorentzian-shaped intrinsic Brillouin gain spectrum given by Eq. (9) and the normalized power spectral density (PSD) of the pump [40]. For the case of a rectangular pulse pump of duration T, the BGS profile can be analytically calculated in a closed-form expression [41]:

$$g_T(\Omega) = g_B(\Omega)\left(1 - \frac{(\Gamma^2+\Omega^2)(1-e^{-\Gamma T}\cos(T\Omega)) + 2\Gamma\Omega e^{-\Gamma T}\sin(T\Omega)}{\Gamma T(\Gamma^2+\Omega^2)}\right) \tag{11}$$

where $\Omega = 2\pi(\nu - \nu_B)$ is the frequency detuning from the BFS, and $\Gamma = \pi\Delta\nu_B \sim 30\pi\ \mathrm{Mrad/s}$ is the half-width at half maximum (HWHM). Expression (11) renders a lower gain peak and broader spectrum profile comparing with the intrinsic Lorentzian profile given by $g_B(\Omega)$ with enhancing spatial resolution improvement.

The corresponding ratio of lowered peak height over the CW-induced peak height can be derived to be:

$$g_{\max} = \left(1 - \frac{1-e^{-\Gamma T}}{\Gamma T}\right) \tag{12}$$

3.3. The crack-induced Brillouin backscattered-light power spectrum based on SGB-FOS

The BFS in the fiber is affected by the strain and temperature, which can be formulated as:

$$\nu_B(T,\varepsilon) = C_\varepsilon(\varepsilon - \varepsilon_0) + C_T(T - T_0) + \nu_{B0}(T_0,\varepsilon_0) \tag{13}$$

When a temperature compensation sensor is presented, the temperature-induced BFS is,

$$\nu_B(T,\varepsilon_0) = C_T(T - T_0) + \nu_{B0}(T_0,\varepsilon_0) \tag{14}$$

Therefore, after temperature compensation, the purely strain-induced Brillouin frequency shift can be obtained,

$$\nu_B(\varepsilon-\varepsilon_0)=\nu_B(T,\varepsilon)-\nu_B(T,\varepsilon_0) \tag{15}$$

where ε and T are the strain and temperature, C_T and C_ε are the temperature and strain coefficients, which are determined by calibration. For standard single-mode fibers using wavelengths around 1550 nm, the near-room temperature C_T are 1 MHz per degree °C, while C_ε 50 MHz per 1000 με. T_0 and ε_0 are the strain and temperature corresponding to the reference Brillouin frequency ν_{B0}, respectively.

The local gain observed at the fiber near end is proportional to the local pump power and the local Brillouin gain coefficient. Specifically, the Brillouin backscattered-light power produced in a small section of the fiber translated by the strain variation detected at an optical receiver is given by:

$$dP_B(z,\nu)=g_T(\nu,\nu_B(\varepsilon-\varepsilon_0))\frac{c}{2n}p(z)e^{-2\alpha z}dz \tag{16}$$

where z = ct/(2n) is distance along the fiber from the light input, p(z) is the launched light power at z, ν is the optical frequency of the Brillouin backscattered light, c is the velocity of light in vacuum, n is the refractive index of the fiber, α is the attenuation coefficient of the fiber, and t is the time interval between the launching of the pulsed light and the detection of the scattered light. Therefore, for any arbitrary given strain distribution within the SR of the analyzer, at the ith measurement z_i,

$$G_i(\nu)=\int_{z_i-SR/2}^{z_i+SR/2} g_T\left\{\nu,\nu_B\left[\varepsilon(z)-\varepsilon_0\right]\right\}\frac{c}{2n}p(z)e^{-2\alpha_z z}dz \tag{17}$$

For a SR << L, power variation due to fiber attenuation within the SR can be neglected, and as we are only interested in the shape change of the spectrum, a normalized spectrum can be obtained as,

$$G_i(v) = \frac{1}{g_{\max}} \int_{z_i - SR/2}^{z_i + SR/2} g_T\left\{v, v_B\left[\varepsilon(z) - \varepsilon_0\right]\right\} dz \tag{18}$$

For our short gauge sensor, under the assumption of rectangular pulsed pump and uniform crack-induced strain, when the background strain variation can be regarded as sufficiently small, the strain distribution within SR at z_i can be expressed as follows:

$$\varepsilon_i(z) = \begin{cases} \varepsilon_c - \varepsilon_0 & (z_i - SR/2) \le z_{lb} \le z \le z_{ub} \le (z_i + SR/2) \\ \varepsilon_0 & (z_i - SR/2) \le z < z_{lb}, z_{ub} < z \le (z_i + SR/2) \end{cases} \tag{19}$$

where z_{lb} and z_{ub} denote the lower and upper boundary of crack-induced strain distribution. Therefore, we can arrive at an approximation of the crack-induced spectrum response in a simple closed form,

$$G_{i,c}(v) = \frac{1}{g_{\max}}\left(\frac{GL_n}{SR}\right) g_T\left(v, v_B\left(\varepsilon_c - \varepsilon_0\right)\right) + \frac{1}{g_{\max}}\left(1 - \frac{GL_n}{SR}\right) g_T\left(v, v_B(\varepsilon_0)\right) \tag{20}$$

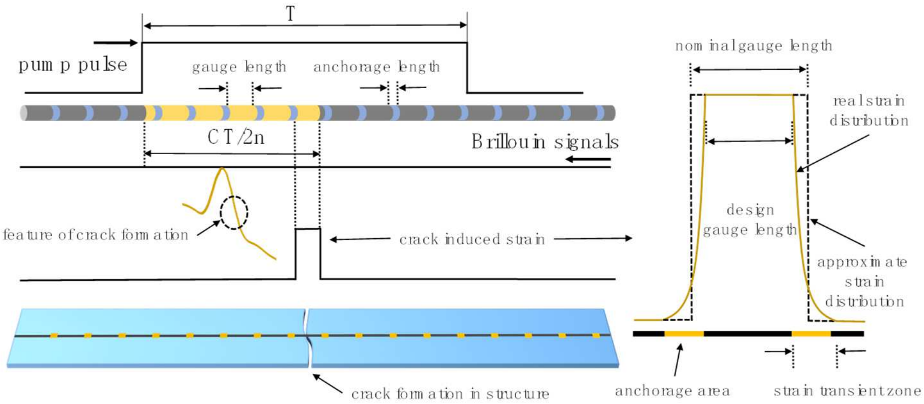

Fig. 4. Schematics of the short gauged Brillouin fiber optic sensor.

3.4. Numerical simulation of the crack-induced BGS response using SGB-FOS

Following the methodologies introduced in section 3.1 to section 3.3, numerical simulation of the BGS evolution using SGB-FOS in response to crack formation can be carried out by implementing the respective formulas in Matlab codes. The following simulation exemplifies the BGS response to crack expansion based on a typical combination of a Brillouin fiber-optic analyzer (560 mm SR) and the SGB-FOS (112 mm GL).

Fig.5(a) demonstrates the predicted BGS evolution of the SGB-FOS corresponding to the varied spectrum of crack-induced strain. We can see that the BGS profile is predicted to change markedly in shape as the crack-induced strain increases. To characterize different spectrum evolutional stages, we extract the peak position from the predicted BGS response demonstrated in Fig.5(a) with the varying crack strain (Fig.5(b)). The BGS peak position is characterized by its frequency shift and power variation compared to its initial position when no crack is present.

In Fig.5(b), it is interesting to note that as the crack strain increases, the BGS peak shifting is predicted to undergo complex nonlinear behavior instead of a simple linear response from the fiber-optic sensors uniformly stressed within the SR of the analyzer. Moreover, the peak power of the BGS is also predicted to evolve nonlinearly with the varying crack-induced strain. Fig.5(b) illustrates the evolution of normalized peak power with varying crack strain. Overall, a three-staged BGS peak-shifting response can be identified. In stage I, the BGS peak begin to shift to higher frequencies with the crack width growth. However, after the peak shifting surpasses a certain level, the trend is reversed, and the peak starts to shift back to its original position as the crack grows. We categorize this reversal-peak-shifting stage as stage II. After this, the peak position becomes relatively stable in response to the increased crack width, undergoing only minor ups and downs. We categorize this as stage III. For peak power evolution, it is noticeable that in stage I and II, the peak power experiences a pronounced decrease. In contrast, the peak power becomes relatively stable when the crack-induced strain enters the stage III region.

In fact, these three stages also characterize the evolutional features of the BGS configuration with different sensitivity to crack width variation. Specifically, when no crack is present, the BGS resembles a Lorentzian curve and is symmetrical against its peak. As small crack forms in stage I, the BGS features a broader spectrum base, asymmetrically leaning leftwards, with a steeper curve slope at its left side in comparison to the right. To illustrate more clearly the characteristic change of the BGS response in stage I, the BGS profiles corresponding to the three representative highlighted crack-induced strain levels in stage I (St.1, St.2, and St.3 in Fig.5(b)) are demonstrated in Fig.5(c). As can be seen, these BGS profiles tend to have a relatively smooth right side curve without localized changes in curvature distribution. During this stage, the characteristics of the BGS configuration undergo no prominent changes as the crack expands, apart from the peak shifting and lowering behaviors, indicating that the BGS shape variation is relatively insensitive to crack expansion at this stage.

In stage II, however, a bump appears rapidly at the high-frequency side of the BGS profile corresponding to the crack expansion, and the configuration of the BGS changes dramatically. Therefore, the occurrence of a bump in the BGS can be served as a clear indicator of crack formation. Two BGS profiles corresponding to the representative crack-induced strain levels in stage II (St.4 and St.5 in Fig.5(b)) are presented in Fig.5(d) to show the corresponding spectrum evolutional process. Obviously, the evolution of the BGS at this stage demonstrates enhanced sensitivity with crack width variation comparing to stage I. In stage III, as the crack further increases in width, the bump formed in stage II is predicted to transform into a separated secondary peak, shedding off from the primary peak. After this, the distance between the secondary and primary peak is predicted to grow in response to further crack width enlargement. One particular BGS profile corresponding to the representative crack-induced strain level in stage III (St.6 in Fig.5(b)) is presented in Fig.5(d) to demonstrate the BGS profile after peak separation when a large crack occurs.

By applying the SGB-FOS, the predicted shape-changing phenomenon of the BGS responding to crack variations demonstrated above can be leveraged for crack detection and potentially its quantification. It is also noticeable that the crack strain corresponding to the peak of the peak-shifting curve (St.3) in Fig.5(b) characterizes the hinge point where prominent changes of the BGS configuration initiate with enlarged crack width, offering a reasonable estimation of the sensor's capability for small crack detection judging on BGS shape only. Bump formation or peak separation in stages II and III can be very straight-forward signs of crack formation. The bump feature is predicted to become very pronounced at the later stage of stage II.

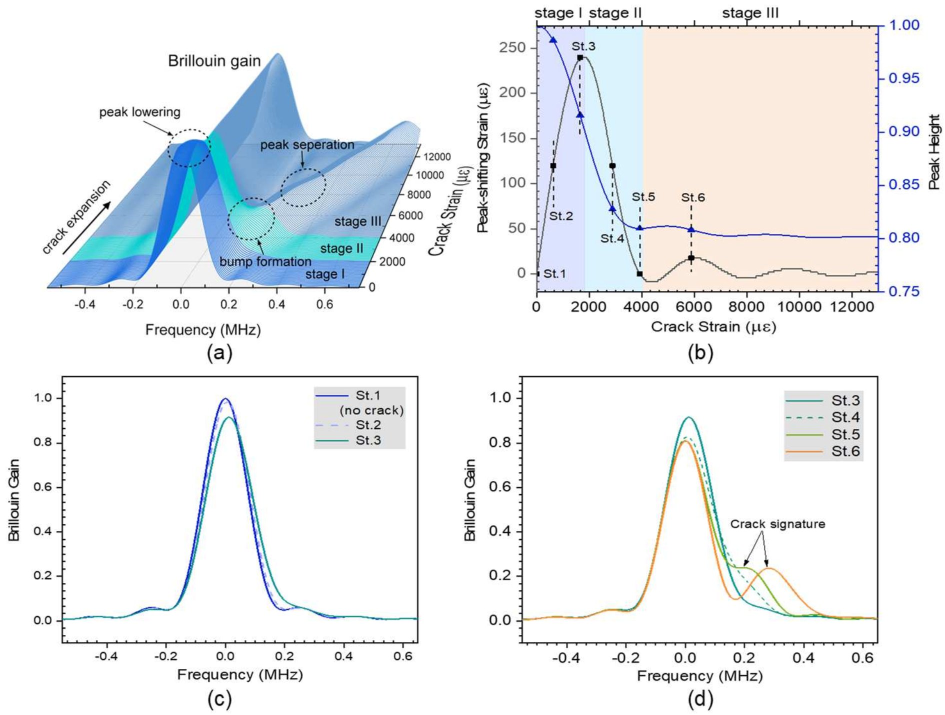

Fig.5. The numerically simulated BGS response to crack expansion using SGB-FOS: (a) BGS evolution with varying crack-induced strain using SGB-FOS of 112 mm GL and Brillouin analyzer of 560 mm SR; (b) BGS peak shifting effect and peak lowering effect (indicated by the normalized peak height) vs different crack-induced strain; (c) simulated BGS response corresponding to selected crack-induced strain in stage I (CS = St.1, St.2, and St.3, respectively); (d) simulated BGS response corresponding to selected crack-induced strain in stage II and III (CS = St.4, St.5, and St.6, respectively).

4. Experimental testing

4.1. Testing setup

To simulate structural crack formation, we deployed two aluminum plates as templates to create a single artificial crack. Each plate spans 1100 mm in length, providing sufficient space to avoid possible interference to the crack-induced signals that may arise due to the distortion effect generated by the strain variations at the plate boundaries. The two plates were bolted to a high-precision fixture frame specifically designed for the fiber optic sensor calibration. SGB-FOSs with the GLs of 60 mm, 90 mm, and 120 mm were installed across the two plates. A tight-buffered fiber optic strain sensing cable of 0.9 mm outer diameter was selected for the assembly of the short-gauged sensor. The fiber optic sensors were glued to the plates by epoxy resin.

The Omnisense DiTeSt BOTDA fiber optic analyzer was used as the interrogation system during the testing, which could reportedly achieve repeatability of ± 2με and spatial resolution as low as 0.5 m. The spatial resolution for the experiment was set to 0.5 m, and the spatial sampling rate was set to every 0.25 m.

Fig.6 shows the design of the testing system. Three displacement gauges with an accuracy of 0.001 mm are placed dispersedly at three different locations along the width of the plates to provide reference measurements for the crack opening.

In the loading stage, the loading system generated an artificial crack by driving the movable plate away from the fixed plate, creating a gap between the two plates. The crack width ranged from 0 mm to 2.0 mm under displacement control during the testing, with increments of 0.025 mm for each step before 0.4 mm and 0.05 mm afterward.

Multiple displacement gauges enabled measuring crack width at different locations along the crack; the crack width measurement from the displacement gauges at each fiber-optic sensor position can be accurately calculated by applying linear regression taken into consideration of the spatial positions of the displacement gauges and the fiber optic sensors.

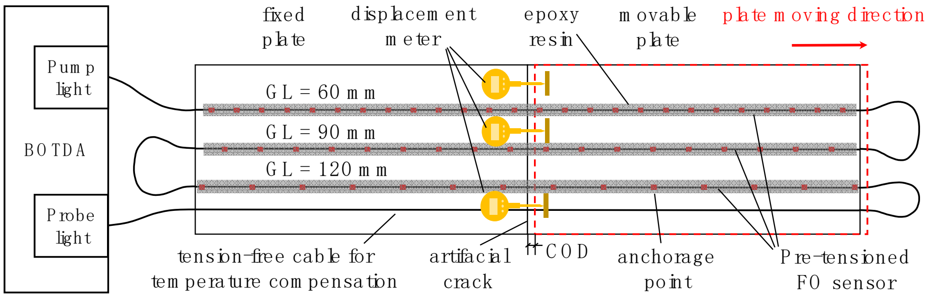

Fig.6. Schematics of the crack-sensing testing using SGB-FOSs

4.2. Verification of the crack-induced BGS response using SGB-FOS

Fig.7 shows the experimental results and the corresponding numerical simulation results according to the methodologies proposed in Section 3 for SGB-FOS with 120 mm GL as an example for comparison. Fig.7(a) and Fig.7(b) present the BGS evolutional process in response to crack expansion. Highly consistent results are obtained in terms of the overall spectrum evolutional pattern between the experimental and simulation results, which confirms the theoretical predictions in Section 3.

Detailed comparisons between the experiment and simulations of the BGS response are demonstrated in Fig.7(c) to Fig.7(h). From Fig.7(c) and Fig.7(d), the peak shifting and peak lowering phenomenon predicted theoretically can be clearly observed in the experimental results. The experimental curves match reasonably well with the simulated results in terms of the evolutional trend. For the peak-shifting behavior shown in Fig.7(c), close consistency between the theoretical and experimental results can be observed for crack expansion in stage I and stage II. Although some discrepancy in magnitude occurs between the experimental and the simulated results for crack expansion in stage III, the two curves still share a very similar trend in the evolutional pattern. We believe the discrepancy is most likely to be caused by the deviation of the actual strain distribution in the fiber optic sensor from the simplified theoretical assumption of a rectangular-shaped crack strain distribution (see Fig.4). The strain transition zone in the sensor's anchorage area inevitably contributes its respective spectrum energy to the measured BGS, which tends to drag the primary peak to a higher frequency even after the secondary peak separation. In contrast, the peak lowering behavior from the experiment matches well with the theoretical prediction in terms of both the overall trend and magnitude (see Fig.7(d)).

Some representative BGS profiles through the crack expansion process are selected for comparison in Fig.7(e) through Fig.7(h). These profiles are the experimental and simulation results that correspond to the crack-induced strains highlighted by colored bars in Fig.7(c) and Fig.7(d), respectively. These spectra demonstrate the entire evolutional process of crack-induced BGS response as the crack expands. The theoretical BGS responses are thus proven to match reasonably well with the experimental results, where the characteristics of the experimentally obtained BGSs are observed to evolve closely as theoretically predicted. Namely, the experimentally obtained BGSs are observed to experience evolutional stages through a process of peak leaning (stage I), bump forming (stage II), and secondary peak separation (stage III).

The consistency between the theoretical and experimental results in various aspects confirms our proposed theoretical framework's suitability to predict the crack-induced BGS response for the SGB-FOSs.

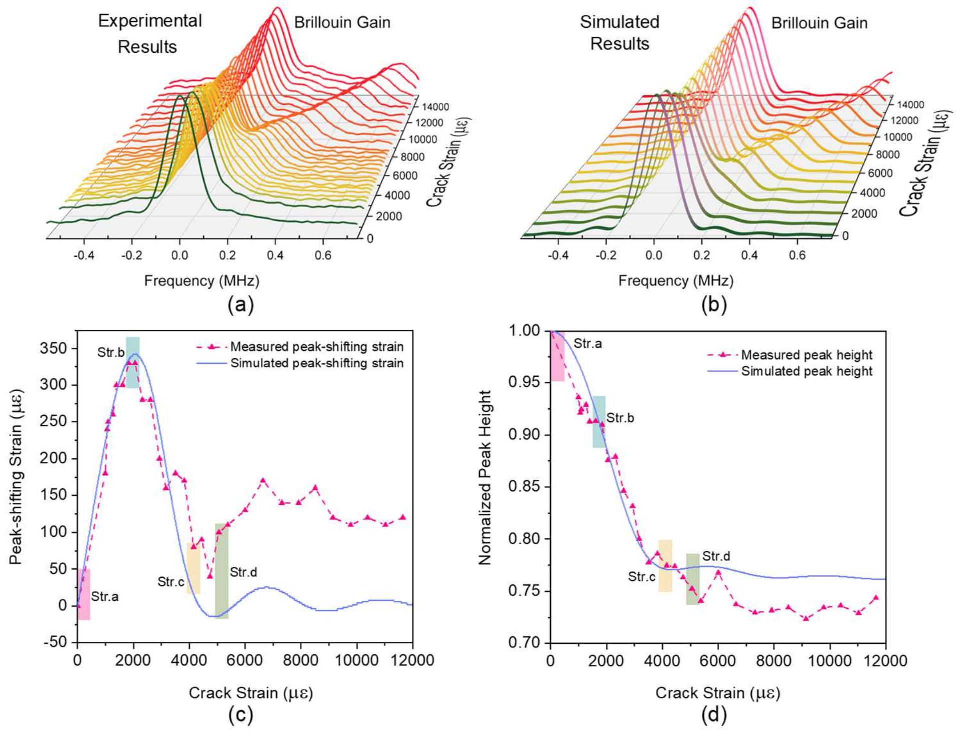

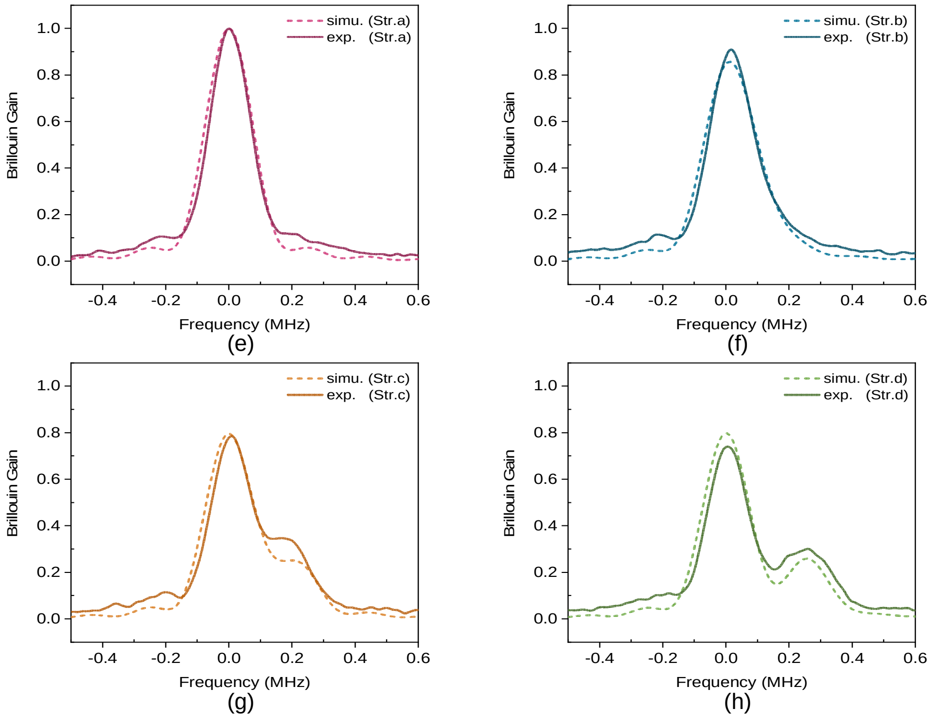

Fig. 7. Experimental and simulated crack-induced BGS response using SGB-FOS: (a) experimental BGS response vs. crack-induced strain (CS); (b) simulated BGS response vs. crack-induced strain; (c) experimental and simulated peak-shifting strain vs. crack-induced strain; (d) experimental and simulated normalized BGS peak height vs. crack-induced strain; (e) experimental and simulated BGS at the crack-free stage (CS = Str.a); (f) experimental and simulated BGS at the end of stage I (CS = Str.b); (g) experimental and simulated BGS at the end of stage II (CS = Str.c); (h) experimental and simulated BGS at stage III (CS = Str.d).

If the SGB-FOSs adopt different gauge lengths, the corresponding crack-induced BGS response will change accordingly. In Fig.8(a) and Fig.8(b), the experimentally obtained BGS evolution using SGB-FOSs in different GLs are shown for comparison. The experimental results suggest that despite different sensor GLs, the BGS evolutional processes share the same evolutional pattern, characterized by a sequential phenomenon that occurs through stage I to stage III as specified in Section 3.4. However, a longer sensor GL means forming a higher and more prominent secondary peak after a particular crack-induced strain is reached. Meanwhile, it also means a more significant peak-lowering behavior. However, SGB-FOSs with a longer GL will render the secondary-primary peak separation to occur later than shorter GLs cases. All these experimental phenomena agree well with the theoretical predictions according to Section 3.

In Fig.8(c) and Fig.8(d), the experimentally obtained BGSs using SGB-FOSs with different GLs at the same evolutional stages are shown for comparison. These experimental results reveal that the crack signatures in the detected BGSs, namely the bump formation and peak separation behaviors, are more prominent for SGB-FOSs with longer GLs. In contrast, shorter GL sensors will render a relatively lower and flatter secondary peak, which can be harder to distinguish due to the influence of intrinsic background noises accompanying the sensing system. Nevertheless, the experimental results suggest that the crack signatures in the BGSs can still be clearly identifiable for the shortest gauge length applied (about 10% of GL/SR ratio).

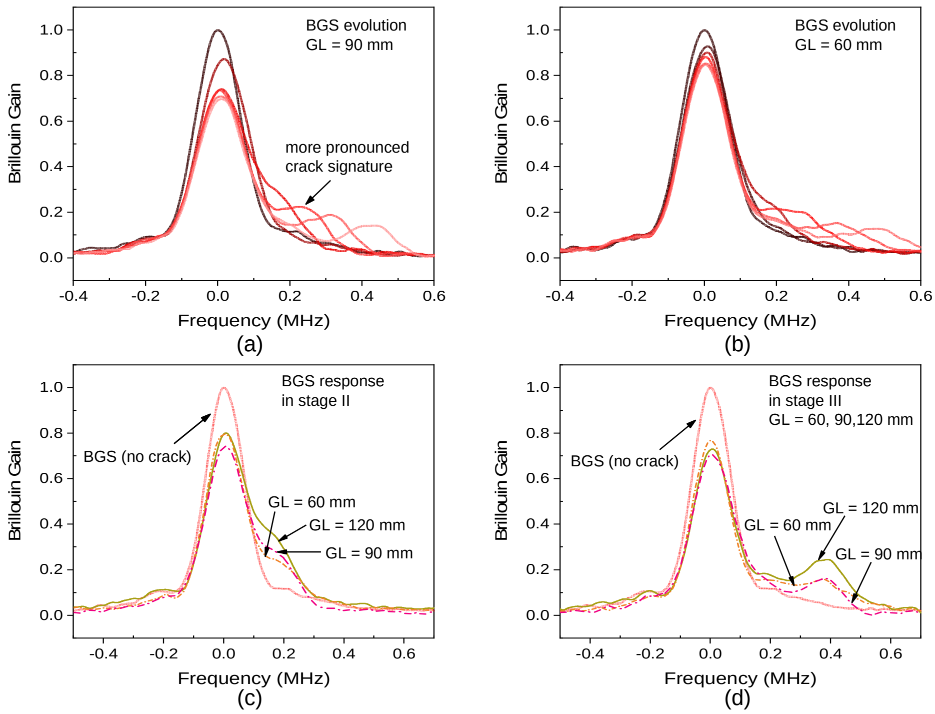

Fig. 8. Experimental results of BGS evolution for SGB-FOSs of different GLs: (a) crack-induced BGS response for SGB-FOS of 90 mm GL; (b) crack-induced BGS response for SGB-FOS of 60 mm GL; (c) stage II crack-induced BGS response for SGB-FOSs with 60 mm, 90 mm, and 120 mm GLs; (d) stage III crack-induced BGS response for SGB-FOSs with 60 mm, 90 mm, and 120 mm GLs.

5. SGB-FOS as distributed crack meter

In the last section, we demonstrate the effectiveness of the theoretical framework in predicting the crack-induced BGS response using the proposed fiber optic sensor. Understandably, the measured BGS configurations contain the crack information, and this could lead to refined quantification of the crack. This section will showcase the possibility of using the SGB-FOS as a distributed crack meter in the engineering practice, enabling retrieval of crack width information via processing the measured BGS data. We also demonstrated in sections 3.4 and 4.2 the possibility of identifying the existence of crack by examining the characteristics of the BGS response. If the crack signatures are observed in the measured BGSs, data processing methodologies can be subsequently applied to obtain the crack width quantitatively.

With the closed-form formulations describing the spectrum’s evolutional process proposed in Section 3, it is theoretically possible to obtain the optimized crack width by matching the theoretical and experimental BGSs through iterative nonlinear curve fitting. However, this approach was found occasionally unstable to reach numerical convergence for some particular measurement datasets. Moreover, it also tends to be computationally expensive to process large datasets.

The adoption of the SGB-FOS enables the resulted BGS response after crack formation to be simplified as a linear superposition of two quasi-Lorentzian curves. According to equation (20), these two quasi-Lorentzian curves differ in power and center frequencies but share the same line width. In view of this, a simplified peak fitting algorithm can be developed to decouple the peak composition in the experimental dataset.

Although a pseudo-Voigt profile was deemed suitable to account for the variations of the BGS arisen from different operating conditions of the sensing systems [42], their usages tend to make the algorithm less stable to reach numerical convergence. Therefore, the peak composition of double Lorentzian curves is assumed for the measured BGS profiles. During the peak decomposition process, an equal-line-width constraint is applied in a peak fitting algorithm written in Matlab codes, reducing the fitting parameters' degree of freedom. As such, the robustness and efficiency of the algorithm are thus enhanced. Reasonable initial values of the peak parameters are appropriately chosen as input for the peak fitting algorithm. Afterward, peak center frequencies and peak heights are obtained by minimizing the discrepancy between the measured BGSs and the composition of fitted peaks through an iterative least-square technique until attaining numerical convergence.

Fig. 9(a) to Fig.9(c) presents the correlation of the crack widths detected by the SGB-FOSs with different GLs through the proposed peak fitting algorithm and the displacement gauge measurements. Test results reveal that all sensors perform excellently in terms of a high degree of linearity for cracks that are relatively large using the peak decomposition algorithm. However, when the crack is relatively small, their quantification can be challenging. A threshold seems to exist below which a high degree of sensor linearity can be hard to achieve. Instead, a small section of nonlinear curves exists before they enter the linear zone. The experimental results suggest that the cracks become measurable when it exceeds a specific value (about 0.1 mm to 0.3 mm), depending on the gauge length adopted. However, before the cracks can be measured with certainty, the peak-leaning phenomenon can already be observed, which can be used as a distinctive sign for identifying early-stage cracks.

To facilitate understanding the reason behind this phenomenon, selected spectrum profiles corresponding to the highlighted points in Fig.9(a) to Fig.9(c) are plotted. We can see that at the early stage of crack formation, as the BGS evolves within stage I, the peak fitting algorithm is not sensitive enough for crack width quantification. However, when the BGS proceeds to stage II and stage III, namely after a bump signature forming clearly in the BGSs, the proposed peak fitting algorithm can effectively retrieve the crack width information with good repeatability and linearity.

Peak fitting results of the selected profiles for the 90 mm GL case (as shown in Fig.9(b)) are illustrated in Fig.9(d) through Fig.9(f) to help understand the performance of the proposed peak fitting algorithm for different stages of BGS response. As shown in Fig.9(e) and Fig.9(f), after apparent secondary peak formation, the peak fitting algorithm renders good fitting results, accurately capturing the secondary peak position, which explains the excellent linearity of the measurement results. However, before the peak separation, the fitting algorithm tends to give larger secondary peak position coordinates than the real value, although the composite curve matches close enough to the measured BGS profile (Fig.9(d)). It appears that direct peak fitting for the early-stage crack-induced BGSs can be susceptible to measurement noises and model discrepancies. Therefore, in this study, we focus our attention on relatively large cracks with relatively prominent crack signatures in the BGS response, such as bump formation and peak separation.

As presented in Fig.9(a) to Fig.9(c), a highly linear correlation is established between the measurement results from the displacement gauges and the fiber optic sensors for crack widths beyond a certain threshold. The corresponding linear regression formulas and the associating R-square values can be derived based on the cases with crack width greater than those thresholds. Those formulas give factors of crack width conversion from the fiber optic sensing systems with different sensor designs. It is noticeable that the factors, calculated by the crack widths detected by the fiber optic sensors over those from the displacement gauges, are always smaller than one. Specifically, for the SGB-FOS of 120 mm GL and the ones of 90 mm GL, the factors are 0.86 and 0.84, respectively. For the SGB-FOS of 60 mm GL, this value declines to 0.69. These factors are, in fact, the characteristic factor k for the particular SGB-FOSs. For sensors with 120 mm and 90 mm GLs, the strain transfer mechanism from the cracked structure to the fiber optic sensor is most likely to be responsible for the discrepancy between the fiber optic measured crack widths and the actual crack widths as has been illustrated in Section 3.1. However, for the 60 mm GL cases, the flattering of the secondary peaks due to the smaller GL/SR ratio seems to render a smaller-biased detected crack width apart from the aforementioned reasons. As shown in Fig.9(g) and Fig.9(h), the relatively low energy of the secondary peak and the low signal-to-noise ratio (SNR) make it more difficult for the peak fitting algorithm to locate the accurate position of the secondary peak. In other words, when the GL/SR ratio for the SGB-FOSs is low, the crack signatures in the BGSs can be blurred by the background noises, and the secondary peak features can become insignificant. In this case, this effect tends to cause the fitted peaks to deviate to the left of where they should be, rendering smaller detected crack widths and thus a lowered crack width conversion factor than the SGB-FOSs with longer GLs.

The linear regression formulas from the sensor calibration tests can be used for crack width quantification in the monitoring practice given a specific SGB-FOS design. From the testing results illustrated in Fig.9(a) to Fig.9(c), the crack only becomes measurable after particular crack width values have been exceeded, and these thresholds relate closely to the GLs of the SGB-FOSs. Different GLs can influence the sensing capability of the crack in two ways. A shorter GL will generate a lower-powered crack signature in the BGS response, which can be more difficult to capture by the peak fitting algorithm, rendering a more challenging crack identification and compromised crack-sensing accuracy. However, a shorter GL would also mean an earlier bump formation in the BGS due to the higher crack-induced strain in the sensor responding to the same crack width, making the BGS more sensitive to the identification of early cracks. The actual performance of the SGB-FOSs for the early crack identification hinges on the comparable influence of these two opposite effects.

These two effects can be demonstrated by Fig.9(a) to Fig.9(c). For SGB-FOS of 120 mm GL, the fiber optic sensor only becomes sensitive to crack greater than 0.3 mm, due to the insignificant bump signature of the BGS at the early phase of the crack formation. To SGB-FOS of 60 mm GL, this value declined to about 0.17 mm, where a sudden jump of fiber-optic detected crack width occurs, indicating the successful identification of the crack signals in the BGS by the peak fitting algorithm. However, the SGB-FOS of 90 mm GL seems to strike a more balanced sensor design, which managed to bring down this threshold to about 0.15 mm for crack identification.

As the test showed that the crack width detected by the SGB-FOSs demonstrated excellent linearity after cracks become measurable, we can evaluate the measurement uncertainty using the deviations of the detected crack width to the respective linear regression values for crack width greater than a certain threshold (the measurable crack widths) for SGB-FOSs of different GLs. Fig.9(i) displayed the measurement error distributions. Comparison between sensors of different GLs suggests that SGB-FOSs with longer GLs tend to possess higher repeatability for crack width measurement. In contrast, measurements from SGB-FOSs with shorter GLs would involve more degrees of uncertainty. The sensor repeatability indicated by two times the standard deviation of the measurement error is estimated to be $\pm$ 0.0154 mm, $\pm$ 0.0248 mm, and $\pm$ 0.0394 mm, for SGB-FOSs with GLs of 120 mm, 90 mm, and 60 mm, respectively.

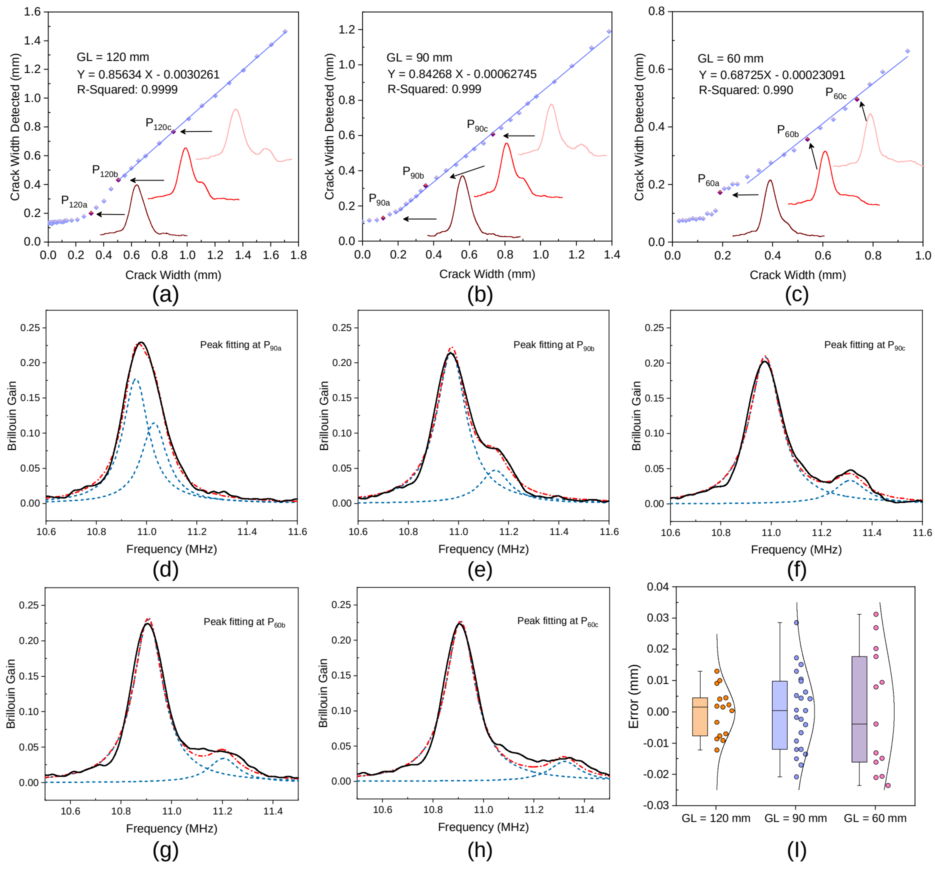

Fig.9. Crack width measurement through peak fitting: (a) crack width from SGB-FOS of 120 mm GL vs that from displacement meters; (b) crack width from SGB-FOS of

90 mm GL vs that from displacement meters; (c) crack width from SGB-FOS of 60 mm GL vs that from displacement meters; (d) peak fitting for SGB-FOS of 90 mm GL at point P_{90a}; (e) peak fitting for SGB-FOS of 90 mm GL at point P_{90b}; (f) peak fitting for SGB-FOS of 90 mm GL at point P_{90c}; (g) peak fitting for SGB-FOS of 60 mm GL at point P_{60b}; (h) peak fitting for SGB-FOS of 60 mm GL at point P_{60c}; (i) error distribution of the crack width measurement for SGB-FOSs of different GLs.

6. Conclusions

This study proposes a novel fiber-optic sensor concept and design called short-gauged Brillouin fiber optic sensor, which enables basic Brillouin-based analyzers to detect and accurately quantify events of cracks or structural discontinuities. As a generic technique, the proposed methodology could potentially facilitate the attainment of long-distance distributed crack sensing and quantification for various civil infrastructures economically.

A sensor example is presented demonstrating the specific design and installation procedures, which are intended to be used for large-scale applications. Theoretical deduction of the BGS transformation for the proposed sensor in response to the expanding crack is established, verified by the laboratory experiment subsequently. Both the theoretical and experimental results identified a three-stage evolutional process of the BGS transformation in response to crack expansion. These stages are categorized by the characteristics of the BGS configurations, peak shifting, and power-lowering behaviors. By observing the presence of these distinctive crack signatures, an early crack warning can be achieved.

Apart from crack detection, the proposed sensor can also become a powerful generic distributed crack meter for different applications, capable of accurate crack-width measurement, minimizing uncertainties that the traditional OB instrumentation approach usually confronts. The adoption of the SGB-FOS enables the development of a simplified peak-fitting-based methodology to extract crack width information within the BGS response robustly and efficiently. The experiment demonstrates the excellent capacity of the proposed sensor to measure cracks with a width greater than a certain threshold, depending on the design GLs of the SGB-FOSs. According to the experimental results, cracks can become measurable as their widths grow greater than around 0.15 mm by the optimized sensors based on the adopted analyzer. Good sensor linearity is achieved for the measurable cracks. Test results suggest that the repeatability of the distributed sensor for crack quantification relies on the sensor gauge length, where smaller gauge sensors tend to be more sensitive to crack width variations but less accurate.

Successful detecting and quantifying cracks in the order of this experiment could carry significant meaning to achieve more advanced infrastructure maintenance systems based on refined structural damage dataset. A crack monitoring system could be made possible, fully aware of the crack distribution and quantification information along the sensor coverage. However, further investigations are required regarding the sensor performance in real-scale infrastructures and the improvement of the sensor's measurement capability for more minor cracks. The proposed technique could be potentially beneficial for preventive structural maintenance of various infrastructures to arrive at decreased life-cycle costs.

Acknowledgements

We would like to thank B.-Y. Yu, Y.Gao, J. Tao, M. Zhang for field support and coordination; C.-Q. Yang, X.-C. Yang, and Z. Zhou for laboratory assistance; and K.Soga for fruitful discussions. We also acknowledge the constructive reviews provided by the Editor and four reviewers. This work was supported by the National Key Research and Development Program of China (2020YFC151190) and the Fundamental Research Funds for the Central Universities.

Conflicts of Interest

The authors declare no conflicts of interest.

Abbreviations

BFS	Brillouin frequency shift	OB	overall bonding
BGS	Brillouin gain spectrum	OTDR	Optical Time Domain Reflectometer
BOTDA	Brillouin optical time-domain analysis	PF	point-fixation
BOTDR	Brillouin optical time-domain reflectometer	PSD	power spectral density
CS	crack-induced strain	RC	reinforced concrete
FOS	fiber optic sensor	SBS	stimulated Brillouin scattering
FWHM	full width at half maximum	SHM	structural health monitoring
GL	gauge length	SNR	signal-to-noise ratio

HWHM	half-width at half maximum	SR	spatial resolution
NDT	non-destructive testing		

References

[1] Y. Yao, S.T.E. Tung, B. Glisic, Crack detection and characterization techniques—An overview, Structural Control and Health Monitoring, 21 (2014) 1387-1413.

[2] G. Sabnavis, R.G. Kirk, M. Kasarda, D. Quinn, Cracked shaft detection and diagnostics: a literature review, Shock and Vibration Digest, 36 (2004) 287.

[3] D. Balageas, X. Maldague, D. Burleigh, V.P. Vavilov, B. Oswald-Tranta, J.-M. Roche, C. Pradere, G.M. Carlomagno, Thermal (IR) and other NDT techniques for improved material inspection, Journal of nondestructive evaluation, 35 (2016) 18.

[4] W. Hong, Z. Wu, C. Yang, C. Wan, G. Wu, Y. Zhang, Condition assessment of reinforced concrete beams using dynamic data measured with distributed long-gage macro-strain sensors, Journal of sound and vibration, 331 (2012) 2764-2782.

[5] B. Wu, G. Wu, C. Yang, Y. He, Damage identification method for continuous girder bridges based on spatially-distributed long-gauge strain sensing under moving loads, Mechanical Systems and Signal Processing, 104 (2018) 415-435.

[6] T. Bao, J. Wang, Y. Yao, A fiber optic sensor for detecting and monitoring cracks in concrete structures, Science China Technological Sciences, 53 (2010) 3045-3050.

[7] K.T. Wan, C.K. Leung, Applications of a distributed fiber optic crack sensor for concrete structures, Sensors and Actuators A: Physical, 135 (2007) 458-464.

[8] N.A. Hoult, O. Ekim, R. Regier, Damage/deterioration detection for steel structures using distributed fiber optic strain sensors, Journal of Engineering Mechanics, 140 (2014) 04014097.

[9] J.-M. Henault, M. Quiertant, S. Delepine-Lesoille, J. Salin, G. Moreau, F. Taillade, K. Benzarti, Quantitative strain measurement and crack detection in RC structures using a truly distributed fiber optic sensing system, Construction and Building Materials, 37 (2012) 916-923.

[10] F. Bastianini, F. Matta, A. Rizzo, N. Galati, A. Nanni, Overview of recent bridge monitoring applications using distributed Brillouin fiber optic sensors, J. Nondestruct. Test, 12 (2007) 269-276.

[11] D. Sigurdardottir, B. Glisic, On-site validation of fiber-optic methods for structural health monitoring: Streicker Bridge, Journal of Civil Structural Health Monitoring, 5 (2015) 529-549.

[12] X. Feng, Y. Han, Z. Wang, H. Liu, Structural performance monitoring of buried pipelines using distributed fiber optic sensors, Journal of civil structural health monitoring, 8 (2018) 509-516.

[13] S. Zhang, B. Liu, J. He, Pipeline deformation monitoring using distributed fiber optical sensor, Measurement, 133 (2019) 208-213.

[14] C.Y. Gue, M. Wilcock, M. Alhaddad, M. Elshafie, K. Soga, R.J. Mair, The monitoring of an existing cast iron tunnel with distributed fibre optic sensing (DFOS), Journal of Civil Structural Health Monitoring, 5 (2015) 573-586.

[15] A. Mufti, D. Thomson, D. Inaudi, H. Vogel, D. McMahon, Crack detection of steel girders using Brillouin optical time domain analysis, Journal of Civil Structural Health Monitoring, 1 (2011) 61-68.

[16] B. Glisic, Y. Yao, Fiber optic method for health assessment of pipelines subjected to earthquake-induced ground movement, Structural Health Monitoring, 11 (2012) 696-711.

[17] M. Niklès, Fibre optic distributed scattering sensing system: Perspectives and challenges for high performance applications, Third European Workshop on Optical Fibre Sensors, International Society for Optics and Photonics, 2007, pp. 66190D.

[18] M.H. Motamedi, X. Feng, X. Zhang, C. Sun, F. Ansari, Quantitative investigation in distributed sensing of structural defects with Brillouin optical time domain reflectometry, Journal of intelligent material systems and structures, 24 (2013) 1187-1196.

[19] X. Feng, X. Zhang, C. Sun, M. Motamedi, F. Ansari, Stationary wavelet transform method for distributed detection of damage by fiber-optic sensors, Journal of Engineering Mechanics, 140 (2014) 04013004.

[20] A. Deif, B. Martín-Pérez, B. Cousin, C. Zhang, X. Bao, W. Li, Detection of cracks in a reinforced concrete beam using distributed Brillouin fibre sensors, Smart materials and structures, 19 (2010) 055014.

[21] F. Ravet, X. Bao, T. Ozbakkaloglu, M. Saatcioglu, Signature of structure failure using asymmetric and broadening factors of Brillouin spectrum, IEEE photonics technology letters, 18 (2006) 394-396.

[22] F. Ravet, X. Bao, Q. Yu, L. Chen, Criterion for subpulse-length resolution and minimum frequency shift in distributed Brillouin sensors, IEEE photonics technology letters, 17 (2005) 1504-1506.

[23] F. Ravet, F. Briffod, B. Glisic, M. Nikle, D. Inaudi, Submillimeter crack detection with Brillouin-based fiber-optic sensors, IEEE Sensors Journal, 9 (2009) 1391-1396.

[24] B. Glisic, D. Inaudi, Development of method for in-service crack detection based on distributed fiber optic sensors, Structural Health Monitoring, 11 (2012) 161-171.

[25] Z. Wu, B. Xu, T. Takahashi, T. Harada, Performance of a BOTDR optical fibre sensing technique for crack detection in concrete structures, Structures and Infrastructure Engineering, 4 (2008) 311-323.

[26] W. Li, X. Bao, Y. Li, L. Chen, Differential pulse-width pair BOTDA for high spatial resolution sensing, Optics express, 16 (2008) 21616-21625.

[27] K. Kishida, C. Li, Pulse pre-pump-BOTDA technology for new generation of distributed strain measuring system, Structural health monitoring and intelligent infrastructure, 1 (2005) 471-477.

[28] T. Sperber, A. Eyal, M. Tur, L. Thévenaz, High spatial resolution distributed sensing in optical fibers by Brillouin gain-profile tracing, Optics express, 18 (2010) 8671-8679.

[29] X. Bao, A. Brown, M. DeMerchant, J. Smith, Characterization of the Brillouin-loss spectrum of single-mode fibers by use of very short (< 10-ns) pulses, Optics letters, 24 (1999) 510-512.

[30] A.W. Brown, B.G. Colpitts, K. Brown, Dark-pulse Brillouin optical time-domain sensor with 20-mm spatial resolution, Journal of Lightwave Technology, 25 (2007) 381-386.

[31] S.M. Foaleng, M. Tur, J.-C. Beugnot, L. Thévenaz, High spatial and spectral resolution long-range sensing using Brillouin echoes, Journal of Lightwave Technology, 28 (2010) 2993-3003.

[32] D. Meng, F. Ansari, X. Feng, Detection and monitoring of surface micro-cracks by PPP-BOTDA, Applied optics, 54 (2015) 4972-4978.

[33] Y. Goldfeld, A. Klar, Damage identification in reinforced concrete beams using spatially distributed strain measurements, Journal of Structural Engineering, 139 (2013) 04013013.

[34] H. Mohamad, K. Soga, P.J. Bennett, R.J. Mair, C.S. Lim, Monitoring Twin Tunnel Interaction Using Distributed Optical Fiber Strain Measurements, Journal of Geotechnical and Geoenvironmental Engineering, 138 (2012) 957-967.

[35] J. Gómez, J.R. Casas, S. Villalba, Structural Health Monitoring with Distributed Optical Fiber Sensors of tunnel lining affected by nearby construction activity, Automation in Construction, 117 (2020) 103261.

[36] M.A. Soto, L. Thévenaz, Modeling and evaluating the performance of Brillouin distributed optical fiber sensors, Optics express, 21 (2013) 31347-31366.

[37] A.W. Brown, M. DeMerchant, X. Bao, T.W. Bremner, Spatial resolution enhancement of a Brillouin-distributed sensor using a novel signal processing method, Journal of lightwave technology, 17 (1999) 1179-1183.

[38] R.W. Boyd, Nonlinear Optics, (2008).

[39] M. Nikles, L. Thevenaz, P.A. Robert, Brillouin gain spectrum characterization in single-mode optical fibers, Journal of Lightwave Technology, 15 (1997) 1842-1851.

[40] E. Lichtman, R.G. Waarts, A. Friesem, Stimulated Brillouin scattering excited by a modulated pump wave in single-mode fibers, Journal of Lightwave Technology, 7 (1989) 171-174.

[41] M. Alem, M.A. Soto, M. Tur, L. Thévenaz, Analytical expression and experimental validation of the Brillouin gain spectral broadening at any sensing spatial resolution, 2017 25th Optical Fiber Sensors Conference (OFS), Ieee, 2017, pp. 1-4.

[42] P. Wait, T. Newson, Measurement of Brillouin scattering coherence length as a function of pump power to determine Brillouin linewidth, Optics communications, 117 (1995) 142-146.